NASA TN D-300

TECHNICAL NOTE

D-300

TEMPERATURE HISTORIES IN CERAMIC-INSULATED HEAT-SINK NOZZLE

By Carl C. Ciepluch

Lewis Research Center
Cleveland, Ohio

NATIONAL AERONAUTICS AND SPACE ADMINISTRATION
WASHINGTON
July 1960

NATIONAL AERONAUTICS AND SPACE ADMINISTRATION

TECHNICAL NOTE D-300

TEMPERATURE HISTORIES IN CERAMIC-INSULATED HEAT-SINK NOZZLE

By Carl C. Ciepluch

SUMMARY

Temperature histories were calculated for a composite nozzle wall by a simplified numerical integration calculation procedure. These calculations indicated that there is a unique ratio of insulation and metal heat-sink thickness that will minimize total wall thickness for a given operating condition and required running time. The optimum insulation and metal thickness will vary throughout the nozzle as a result of the variation in heat-transfer rate. The use of low chamber pressure results in a significant increase in the maximum running time of a given weight nozzle.

Experimentally measured wall temperatures were lower than those calculated. This was due in part to the assumption of one-dimensional or slab heat flow in the calculation procedure.

INTRODUCTION

One approach to providing exhaust nozzles suitable for long-burning-time, high-performance solid-propellant rockets is to insulate the nozzle with a high-temperature ceramic coating. Successful ceramic coatings have been the object of much research and development over the past 10 to 15 years. A helpful contribution to this continuing effort would be an analysis of the heat flow and temperature gradient through composite walls for different operating conditions and composite wall proportions. An analysis of this type can establish the limits of usefulness of ceramic coatings. Accordingly, temperature-time histories were computed in a ceramic-coated metal-base composite wall by a numerical integration procedure. Temperature-time histories in a ceramic-coated nozzle were obtained experimentally on a solid-propellant rocket in order to check the calculations.

In the analytical study the effects of coating thickness, metal-base thickness, and chamber pressure on the maximum running time for a composite wall were determined. The maximum running time was determined by limiting the local ceramic and metal temperatures to values lower than their melting points.

Experimental temperature-time histories of the metal section of the composite wall were determined for several chamber pressures and nozzle area ratios. A comparison of the agreement between the experimental and analytical temperature-time histories was made.

APPARATUS AND PROCEDURE

Motor

A photograph of the solid-propellant rocket motor installation is shown in figure 1. The propellant was a composite, end-burning grain that was inhibited at the head end and circumferentially. An insulating sleeve was used to protect the chamber walls. The calculated gas equilibrium chamber properties were as follows:

Temperature, $^{\circ}R$	5122
γ	1.164
c_p, Btu/(lb)($^{\circ}F$)	0.676
c^*, ft/sec	4861
Gas composition, mol percent	
Cl	0.7
H	.3
CO	11.2
CO_2	11.6
H_2	5.5
H_2O	39.4
HCl	20.8
N_2	9.0
NO	.1
O_2	.1
OH	1.5

Nozzle

A cross-sectional view of the nozzle geometry used in the experimental investigation is shown in figure 2. The nozzle consisted of a copper insert at the throat and a steel divergent section. The nozzle throat area was varied by modifying the copper insert and the divergent section of the nozzle. Internal surfaces of the nozzle were sand-blasted, "flame sprayed" with a thin (0.005 in. or less) coating of Nichrome, and then "flame sprayed" with zirconium oxide; the latter coating was sanded to make the surface and thickness more uniform.

Instrumentation

Transient measurements of chamber pressure and wall temperatures were recorded with a high-speed direct-recording oscillograph. Chamber-pressure static taps located just ahead of the nozzle measured essentially total chamber pressure. The method of installing wall thermocouples is illustrated in figure 2. Temperature measurements were made at nominal area ratios of 4.5 and 7.5. No temperature measurements were made in the thin ceramic-insulation coatings. Chamber-pressure and temperature measurements were accurate to ±1 percent.

Procedure

The weight of solid propellant burned was determined by weighing the motor before and after firing. Firings were made at several chamber pressures by varying the nozzle throat diameter. The measured metal wall-temperature histories were compared with those calculated for the same operating conditions. Symbols are defined in appendix A, and the method of calculating transient wall temperatures is presented in appendix B. Calculated values of the heat-transfer coefficient and the gas temperature were determined as described in appendix C. The ceramic-coating and metal-wall thicknesses were measured before and after each run in the areas where instrumentation was located. There was no measurable erosion of the coating. The accuracy of the ceramic-coating measurements was limited to ±5 percent because of the inherent roughness of the coating.

RESULTS AND DISCUSSION

Factors Affecting Design of Ceramic-Insulated Nozzles

An illustration of typical temperature histories calculated for a steel wall insulated with zirconium oxide at the nozzle throat is shown in figure 3. The insulation surface, interface, and metal cold surface temperatures are plotted against time for a 400-pound-per-square-inch-absolute chamber pressure. The rate of rise of the insulation surface temperature is very high at first and then abruptly decreases. The primary reason for the decrease is that the high surface temperature reduces the heat transferred to the wall by decreasing the temperature difference between the gas and the wall. The quantity of heat that can be absorbed by the metal heat sink then determines the rate of insulation temperature rise.

Optimization of insulation and metal thicknesses. - Since the heat absorbed by the nozzle wall is proportional to the temperature difference between the gas and nozzle wall, the higher the insulation surface temperature, the greater the reduction in absorbed heat. However, because

the melting temperature of ceramic insulating coatings is usually less than the flame temperature of high-performance propellants, the insulation temperature must be limited if severe erosion is to be avoided. Likewise, the metal base has a maximum temperature limit due to strength considerations. Therefore, in order to keep the nozzle weight to a minimum and stay within safe temperature limits on both insulation and metal, the insulation and metal thicknesses must be selected carefully for a given operating condition.

An example of the effect of insulation and metal-base thickness on running time for the nozzle throat was calculated and is shown in figure 4 for a chamber pressure of 400 pounds per square inch absolute and a gas temperature of 4660° F. The calculations were made for a composite wall consisting of zirconium oxide insulation (melting temp. 4500° F) on a mild-steel base. The limiting temperatures of the zirconium oxide and steel were taken to be 4100° and 1800° F, respectively. It can be seen that there is a well-defined optimum value of insulation-coating thickness that results in a maximum running time for each wall size. This is a result of the limiting temperatures of both the insulation and metal base. At the peak of each curve, both the insulation and the metal are locally at their limiting values. For larger than optimum insulation percentage, the insulation temperature reaches its limiting value first, while the metal temperature is limiting for insulation percentage less than optimum. It can also be seen that maximum nozzle life increases with increasing wall thickness or heat sink. However, the increase is not proportional to the wall thickness, because the larger temperature gradient that exists with heavier walls results in a lower average wall temperature, and the heavier wall is therefore a less efficient heat sink. The curves in figure 4 apply only to conditions at the nozzle throat. Primarily as a result of the variation in convective heat-transfer coefficient, the optimum required metal heat sink and insulation thickness will also vary through the nozzle. It is therefore necessary that the optimum proportion between insulation and metal thicknesses be determined at several points to minimize the wall weight along the entire nozzle.

Effect of chamber pressure on maximum running time. - The rate of heat transferred to the nozzle walls directly affects the running time of a given nozzle. One of the important factors affecting heat-transfer rate over which the designer has some control is the chamber pressure. The convective heat-transfer coefficient and the chamber pressure are related approximately as follows:

$$h_f \approx p_c^{0.8}$$

The use of low chamber pressures is then a means of reducing the heat-transfer rate and increasing the running time of heat-sink nozzles. An example of the effect of chamber pressure on maximum nozzle running time

calculated for a nominal 0.4-inch composite wall, nozzle throat conditions, and a propellant gas temperature of 4660° F is shown in figure 5. The maximum nozzle running time was determined by optimizing the insulation thickness at each chamber pressure while holding the nozzle wall weight per unit area constant. This allowed the zirconium oxide insulation and steel base to reach their maximum limits of 4100° and 1800° F, respectively. It can be seen in figure 5 that, for low-chamber-pressure operation, very long running times are possible; while at high chamber pressures running time is severely limited. For example, a running time of 105 seconds was calculated for a chamber pressure of 50 pounds per square inch absolute, while at 1000 pounds per square inch absolute a running time of only 6.5 seconds is possible. While this trend results primarily from the reduced heat-transfer rate at lower chamber pressures, a second benefit is that a lower heat-transfer rate reduces the temperature gradient in the nozzle wall, resulting in more effective use of the metal heat sink. It is also apparent that the optimum insulation and metal thicknesses are affected by variation in chamber pressure. The insulation layer comprises 45.83 percent of the wall thickness at 50 pounds per square inch absolute and only 4.50 percent at 1000 pounds per square inch absolute.

While reductions in chamber pressure permit longer nozzle running times for a given wall weight per unit area, motor thrust is reduced. In order to keep motor total impulse constant (thrust multiplied by running time equals a constant), lower-chamber-pressure operation requires compensating increases in running time or nozzle throat area or a combination of both. Increased nozzle throat area also results in a small reduction in heat transferred to the nozzle due to reduced convective heat-transfer coefficients. It can be shown that the weight of a heat-sink nozzle for high-chamber-pressure operation will be approximately the same as for a low-chamber-pressure nozzle with increased throat area and running time to maintain constant total impulse. The advantage of low-chamber-pressure operation lies in the fact that a much greater range of running time is available for a required total impulse. It should be pointed out that low-chamber-pressure operation is best suited to high-altitude applications, since here the nozzle thrust coefficient is relatively unaffected by the resulting reduction in nozzle pressure ratio.

Comparison of Calculated and Experimental Temperature Histories

In order to determine how well the calculation procedure can predict temperatures in composite walls, experimental wall temperature measurements were made on a ceramic-insulated steel nozzle during solid-propellant rocket firings and were compared with calculated values. Experimental temperature histories were obtained from fine thermocouples that were imbedded in the metal portion of the nozzle. The method of calculating average experimental heat-transfer coefficients and effective

combustion temperature is described in appendix C. A comparison of a number of experimental and calculated temperature histories for the steel section of the composite wall at nominal area ratios of 4.5 and 7.5 and at several chamber pressures is shown in figure 6. Examination of the temperature histories indicates that for all cases the measured metal temperatures were lower than those calculated. The measured temperature rise for all the data varied from 71 to 86 percent (an average of 78 percent) of the calculated temperature rise at the end of the run. A primary reason that the ratio of the measured to calculated temperature rise varied from run to run was that the measurement of the insulating-coating thickness was only accurate to ±5 percent.

One source of discrepancy between the measured and calculated temperatures was the assumption of one-dimensional (slab) heat flow. This is due to the fact that the annular nozzle wall has a larger cross-sectional area (or heat sink) than a flat wall of the same thickness. The effect of the assumption of slab heat flow on wall temperature can be estimated by assuming that local wall temperature is an inverse function of the wall cross-sectional area or,

$$\frac{t_{slab}}{t_{annular}} \approx \frac{A_{annular}}{A_{slab}}$$

and, if d_o and d_{in} are the outside and inside diameter of an annular wall,

$$\frac{A_{annular}}{A_{slab}} = \frac{1}{2}\left(\frac{d_o}{d_{in}} + 1\right)$$

Applying this approximation to the data from figure 6, the difference between slab and annular heat flow accounts for about 5 to 10 percent of the calculated temperatures. If the calculated temperatures are corrected to represent annular heat flow, the measured temperature then averages about 86 percent of the calculated temperature rise.

Another factor that contributed to the difference between measured and calculated temperatures was the use of an end-burning solid-propellant grain to obtain the experimental temperature histories. The measured wall temperatures were probably decreased as a result of the local cooling effect due to evaporation and ablation of the inhibitor and case insulation that encased the propellant grain.

SUMMARY OF RESULTS

1. Calculation of typical temperature histories in ceramic-insulated heat-sink nozzles indicated that there is a distinct optimum insulation

and metal heat-sink thickness that will minimize total wall thickness for a given operating condition and required running time. This optimum exists when safe operating temperature limits are imposed on the insulation and metal. The optimum insulation and metal thicknesses will vary throughout the nozzle as a result of variation in heat-transfer rate.

2. Reducing the chamber pressure results in a significant increase in the maximum running time of a given weight nozzle. Chamber pressure affects the optimum insulation and metal thicknesses.

3. Comparison of experimental and calculated wall temperature histories showed that the measured temperatures averaged about 78 percent of the calculated temperatures for slab heat flow, and about 86 percent of the estimated temperature for annular heat flow.

Lewis Research Center
National Aeronautics and Space Administration
Cleveland, Ohio, April 29, 1960

APPENDIX A

SYMBOLS

A	area, sq in.
c^*	characteristic velocity, ft/sec
c_p	specific heat at constant pressure, Btu/(lb)(^oF)
d	diameter, in.
d_o/d_{in}	ratio of nozzle outside to inside diameters
h_f	convective heat-transfer coefficient, Btu/(hr)(sq ft)(^oF)
k	thermal conductivity, Btu/(hr)(sq ft)(^oF/in.)
M	dimensionless parameter, $M = \Delta x^2/(\alpha \Delta\tau)$
N	dimensionless parameter, $N = h_f \Delta x/k$
n	number of slabs or increments
Pr	Prandtl number
p_c	chamber pressure, lb/sq in. abs
q	quantity of heat transferred, Btu/hr
R	dimensionless parameter, $R = \Delta x_i k_m/\Delta x_m k_i$
Re	Reynolds number
t	temperature, ^oF
t_e	temperature at end of last wall increment, ^oF
t_f	film temperature, ^oF
t_R	adiabatic wall recovery temperature, ^oF
t_o	surface temperature, ^oF
w	flow rate, lb/sec
x	thickness, in.

Δx	incremental wall thickness, in.
α	thermal diffusivity, sq ft/hr
γ	ratio of specific heats
μ	viscosity
τ	time, sec
$\Delta\tau$	time increment, sec

Subscripts:

f	film
i	insulation
int	interface between metal and insulation
m	metal
s	static
t	throat
w	wall
1,2,3,...	center of wall incremental thickness

APPENDIX B

METHOD OF CALCULATING TEMPERATURE TRANSIENTS IN COMPOSITE WALLS

A simplified numerical integration method was used to calculate temperature-time histories in a composite wall, using a high-speed digital computer. The method was based on the numerical method for calculating one-dimensional transient heat conduction and storage described in reference 1. In this numerical integration procedure, the composite wall is divided into a number of increments Δx or slabs, as indicated in the following sketch:

Composite wall cross section

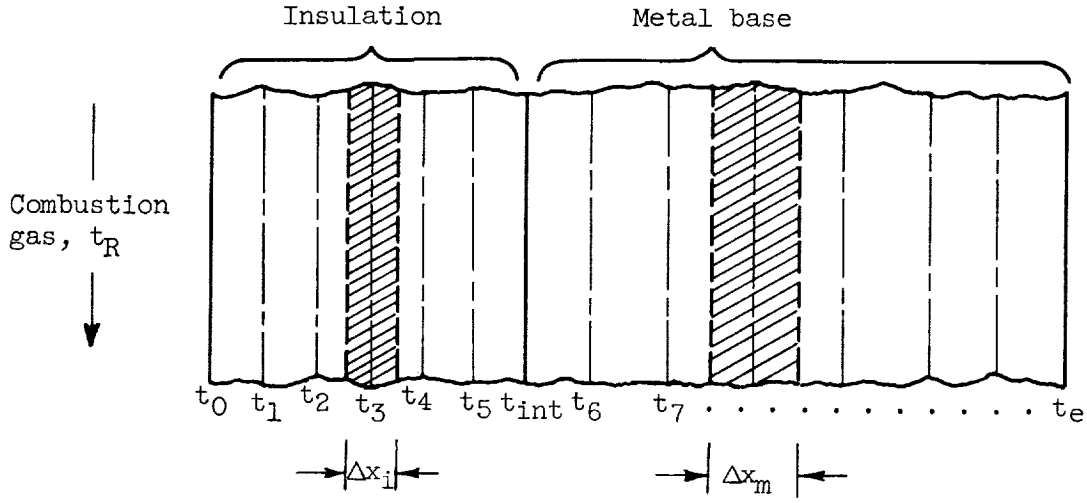

The temperature rise of a slab resulting from the heat absorbed during a finite period of time $\Delta\tau$ is found by making a heat balance:

$$\text{Heat absorbed by slab} = q_{\text{entering}} \times \Delta\tau - q_{\text{leaving}} \times \Delta\tau$$

where

$$q = kA(dt/dx)$$

and dt/dx, the temperature gradient between adjacent slabs, is approximated by assuming that the wall temperature between adjacent slabs varies linearly with x.

Equations for transient conduction through a composite wall can be derived from the preceding heat balance. A detailed derivation of equations will not be presented here but is available in reference 1 or 2.

The general form of the equations used to calculate temperatures at various points in the composite wall is as follows:

I. The surface temperature t'_0 is given by

$$t'_0 = \frac{2Nt_R + [M_i - (2N + 2)]t_0 + 2t_1}{M_i}$$

where the primed temperatures represent the temperature after an elapsed time $\Delta\tau$. The value of M_i was chosen so that $M_i > 2N + 2$ in order that t_0 would not exert a negative influence on t'_0. The convective heat-transfer coefficient, which is contained in the parameter N, was found using the equation (ref. 2) $h_f = 0.023(k/d)Re^{0.8}Pr^{0.33}$, where all fluid properties were evaluated at the film temperature $[t_f = (t_s + t_w)/2]$.

II. In the insulation layer

$$t'_{1,2,3,4,5} = \frac{t_{n-1} + (M_i - 2)t_n + t_{n+1}}{M_i}$$

III. At the interface between insulation and metal

$$t'_{int} = \frac{t_{int-1} + \left(\frac{M_i}{2} + \frac{M_m R}{2} - 1 - R\right)t_{int} + Rt_{int+1}}{\frac{M_i}{2} + \frac{M_m R}{2}}$$

In this equation a choice of M_m must be made, and there are several restrictions governing this choice. The time increments must be equal $(\Delta\tau_i = \Delta\tau_m)$ in order to pass continuously in time increments from the insulation into the metal, and secondly the metal slab thickness Δx_m should be integral with the metal thickness x_m. Therefore, in the equation for M_m,

$$M_m = \frac{(\Delta x_m)^2}{\alpha_m \Delta\tau_m} = \frac{(x_m/n_m)^2}{\alpha_m \Delta\tau_m}$$

a number of slabs n_m was selected that made M_m equal to or slightly greater than M_i.

IV. In the metal section

$$t'_{6,7,\ldots} = \frac{t_{n-1} + (M_m - 2)t_n + t_{n+1}}{M_m}$$

V. The equation for calculating t'_e was

$$t'_e = \frac{2t_{e-1} + (M_m - 2)t_e}{M_m}$$

The preceding calculation procedure has several assumptions or limitations:

(1) One-dimensional heat flow (slab flow)

(2) All heat absorbed in wall (perfectly insulated)

(3) Constant average thermal diffusivity of insulation and metal

(4) Constant average gas film heat-transfer coefficient

To begin the calculation procedure, an average surface temperature was assumed, and the convective heat-transfer coefficient was evaluated. An assumption of the average thermal diffusivity of the insulation and metal was then made. A choice of the number of insulation increments or slabs was made, and the dimensionless parameters N and M were then evaluated. The use of a large number of slabs improves the accuracy of the calculations, however, at the expense of an increase in the time required to calculate the problem. The calculation procedure was repeated until the assumed surface temperature and thermal diffusivities agreed with the calculated values.

APPENDIX C

METHOD OF CALCULATING EXPERIMENTAL VALUES OF LOCAL HEAT-TRANSFER COEFFICIENT

One of the requirements necessary to calculate local heat-transfer coefficients is the knowledge of the effective flame temperature. The theoretical flame temperature was evaluated for the solid propellant used in the experimental investigation in the manner described in references 3 and 4. The effective flame temperature was found by correcting the theoretical flame temperature for combustion inefficiency:

$$t_{effective} = t_{theor.} \left(\frac{c^*_{measured}}{c^*_{theor.}} \right)^2$$

The recovery temperature was

$$t_R = t_s + 0.9(t_{effective} - t_s)$$

Local values of the gas film heat-transfer coefficient were calculated using the following general relation:

$$h_f = 0.023(k/d)Re^{0.8}Pr^{0.333}$$

(ref. 2) where all properties were evaluated at the film temperature $t_f = (t_s + t_w)/2$. By substituting and combining terms, the preceding equation can be rearranged into the following form:

$$h_f = 0.023 \frac{c_{p,f}\mu_f^{0.2}}{d^{0.2}Pr_f^{0.67}} \left(\frac{\dot{w}}{A} \frac{t_s}{t_f} \right)^{0.8}$$

The values of μ, k, and Pr in this equation were estimated using the data from reference 5. The value of $\dot{w}/A$, the rate of propellant flow per unit flow area, was determined in the following manner. The instantaneous propellant flow rate for a solid-propellant motor can be approximated very closely by

$$\dot{w} = \frac{wp_c}{\int p_c \, dt}$$

where w is the total propellant weight burned, p_c is the chamber pressure, and $\int p_c \, dt$ is the area under the chamber-pressure trace. An average value of $\dot{w}$ for the time interval from ignition to tailoff was determined by substituting an average value of chamber pressure for the same time interval into the preceding equation. The value of heat-transfer coefficient calculated by this procedure is therefore an average value for the time interval from ignition up to but not including tailoff.

REFERENCES

1. Dusinberre, G. M.: Numerical Methods for Transient Heat Flow. Trans. ASME, vol. 67, no. 8, Nov. 1945, pp. 703-710; discussion, pp. 710-712.

2. McAdamas, William H.: Heat Transmission. Third ed., McGraw-Hill Book Co., Inc., 1954.

3. Huff, Vearl N., Gordon, Sanford, and Morrell, Virginia E.: General Method and Thermodynamic Tables for Computation of Equilibrium Composition and Temperature of Chemical Reactions. NACA Rep. 1037, 1951. (Supersedes NACA TN's 2113 and 2161.)

4. Gordon, Sanford, Zeleznik, Frank J., and Huff, Vearl N.: A General Method for Automatic Computation of Equilibrium Compositions and Theoretical Rocket Performance of Propellants. NASA TN D-132, 1959.

5. Hirschfelder, Joseph O., Curtiss, Charles F., and Byrd, R. Byron: Molecular Theory of Gases and Liquids. John Wiley & Sons, Inc., 1954.

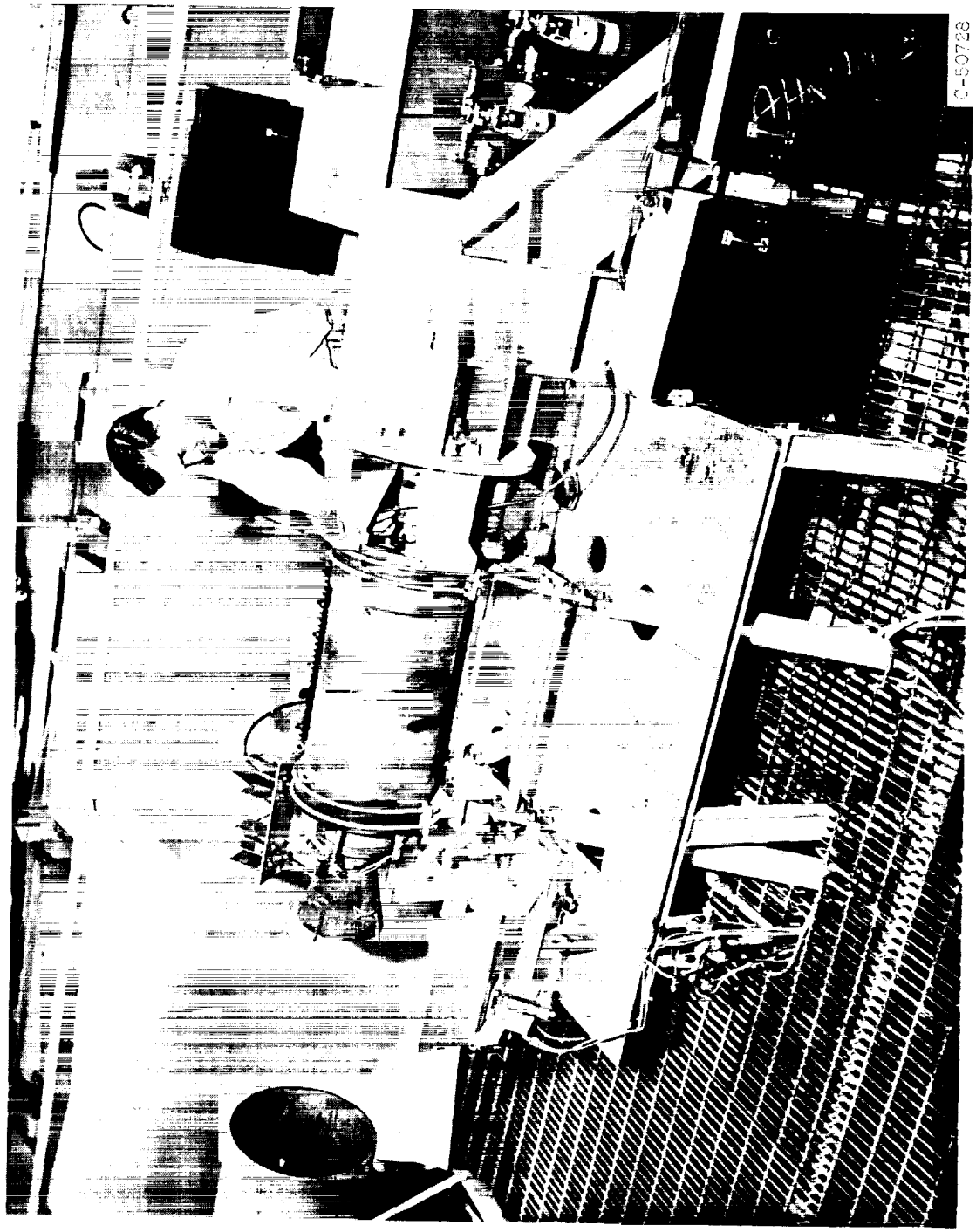

Figure 1. - Motor installation.

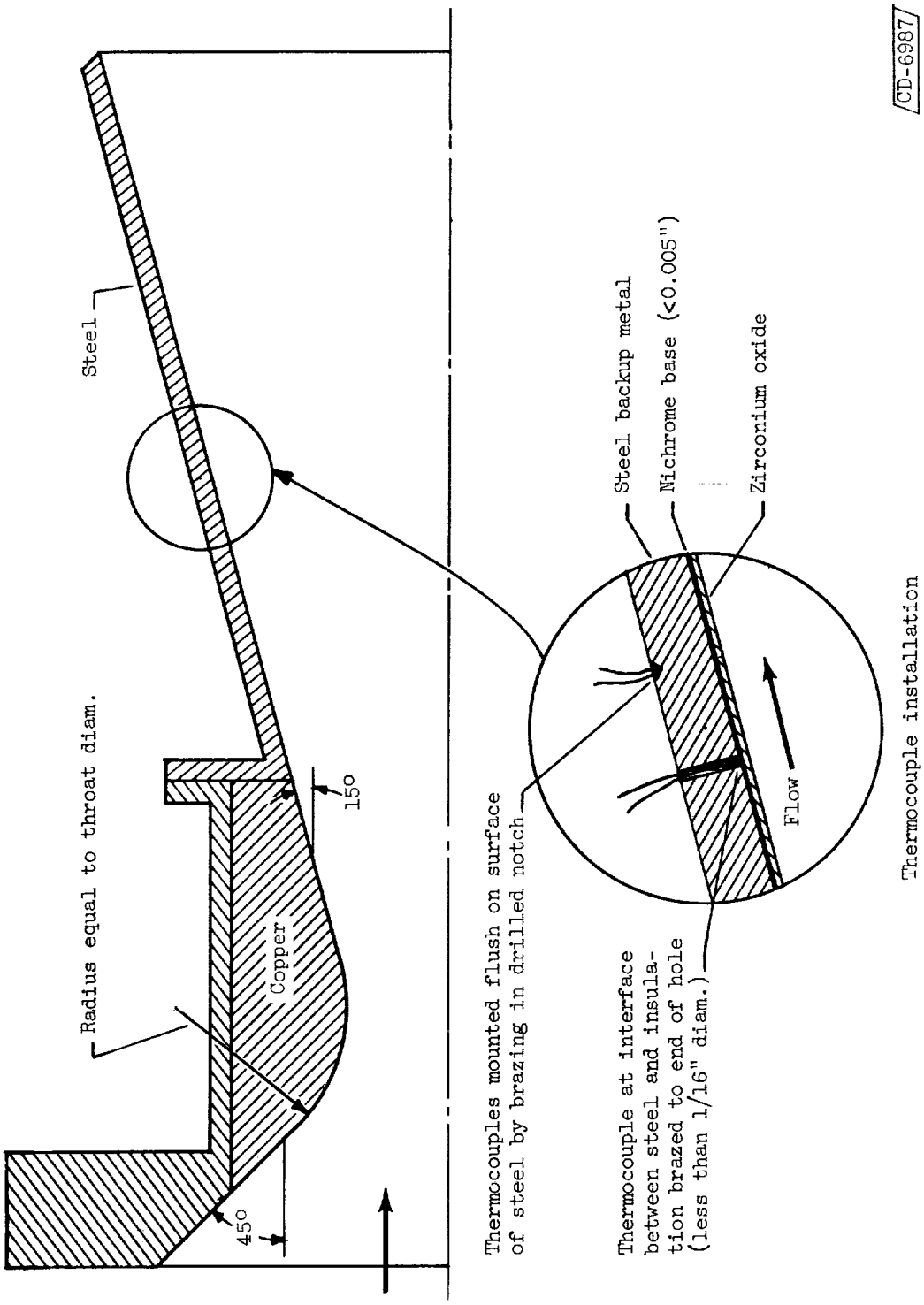

Figure 2. - Cross section of nozzle and thermocouple details.

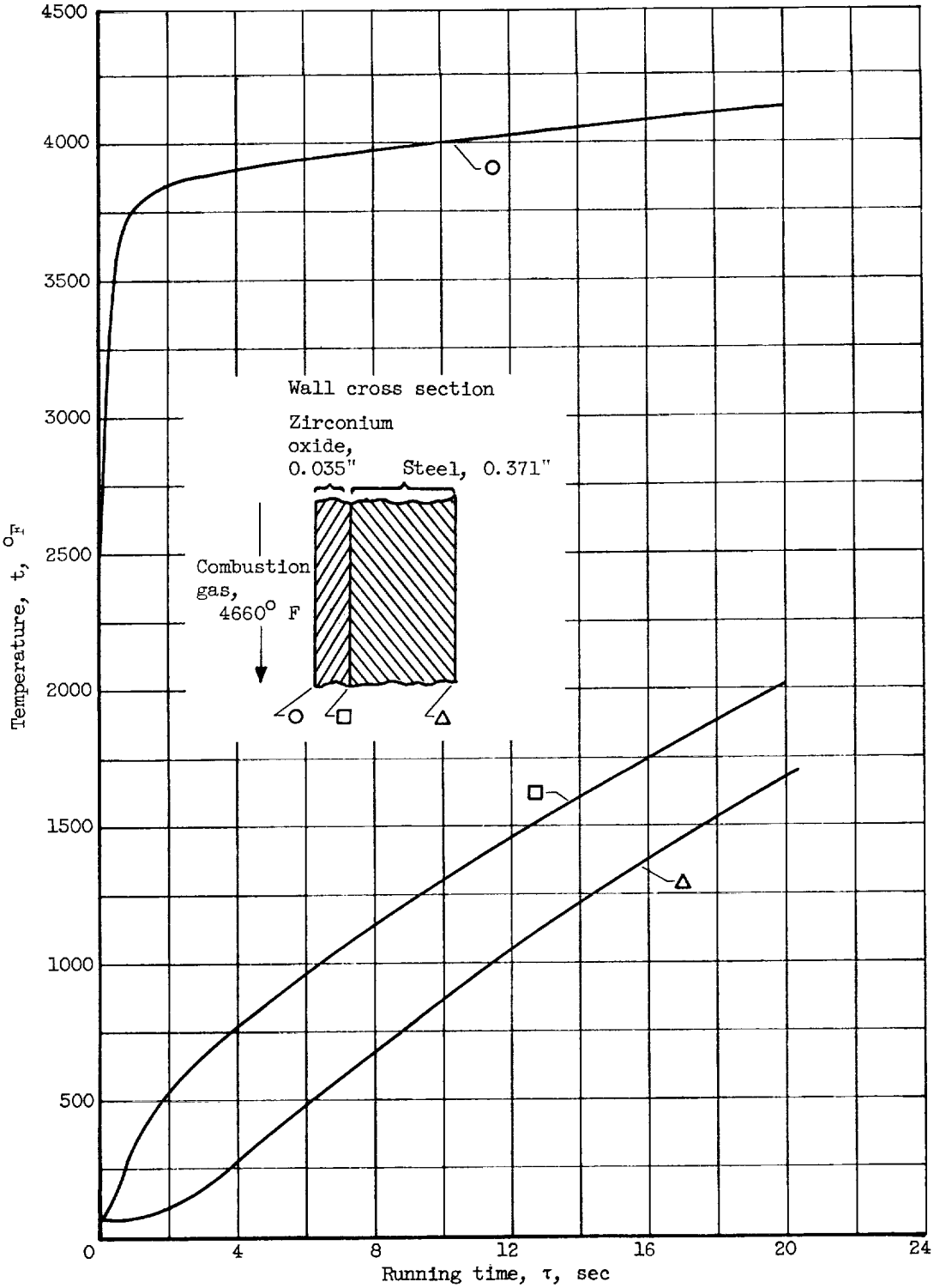

Figure 3. - Typical calculated temperature histories for composite wall at nozzle throat.

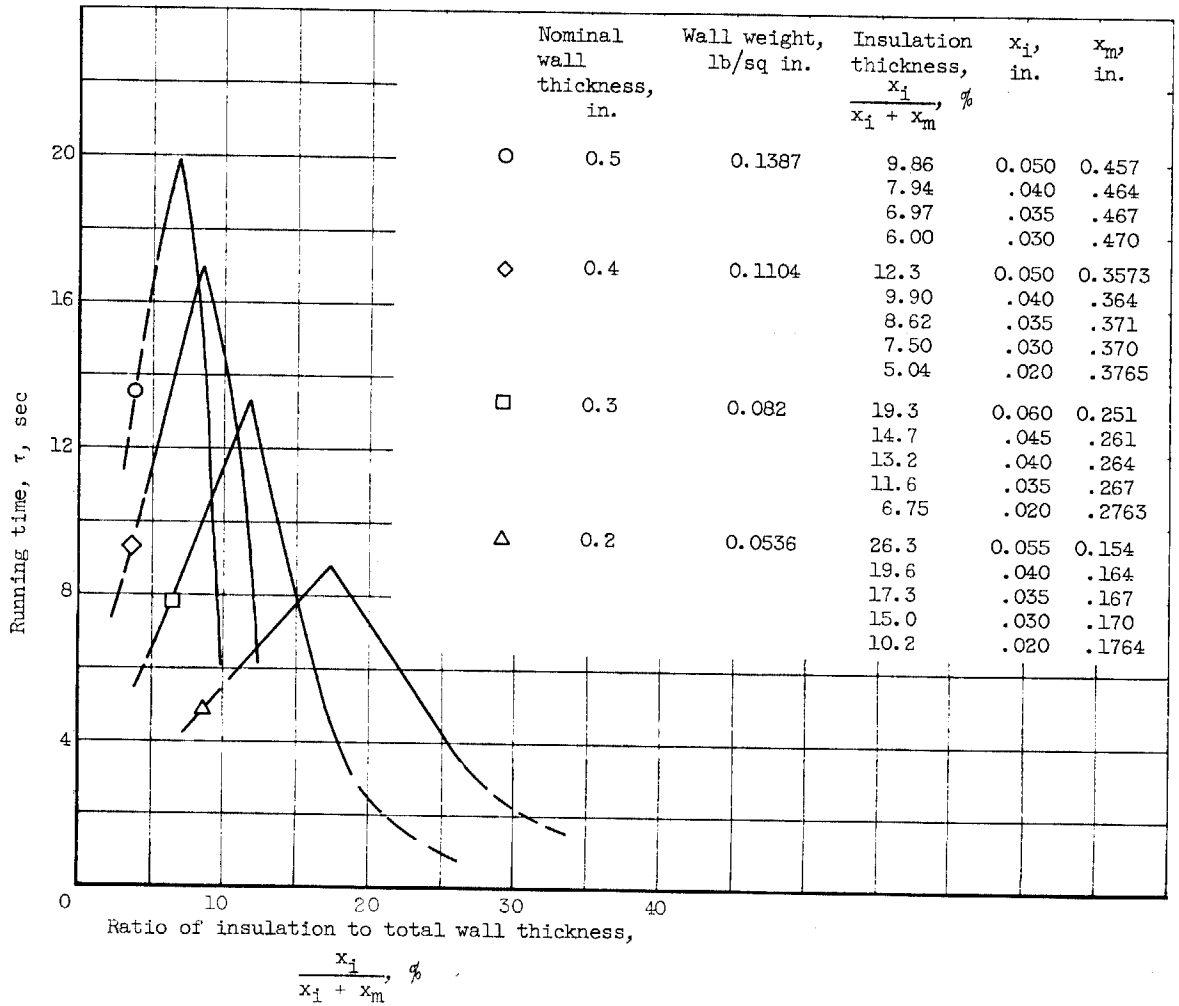

Figure 4. - Calculated effect of insulation thickness and total wall thickness on nozzle throat running time. Maximum temperature limits of 4100° and 1800° F on ceramic coating and metal base. Chamber pressure, 400 pounds per square inch absolute; gas temperature, 4660° F.

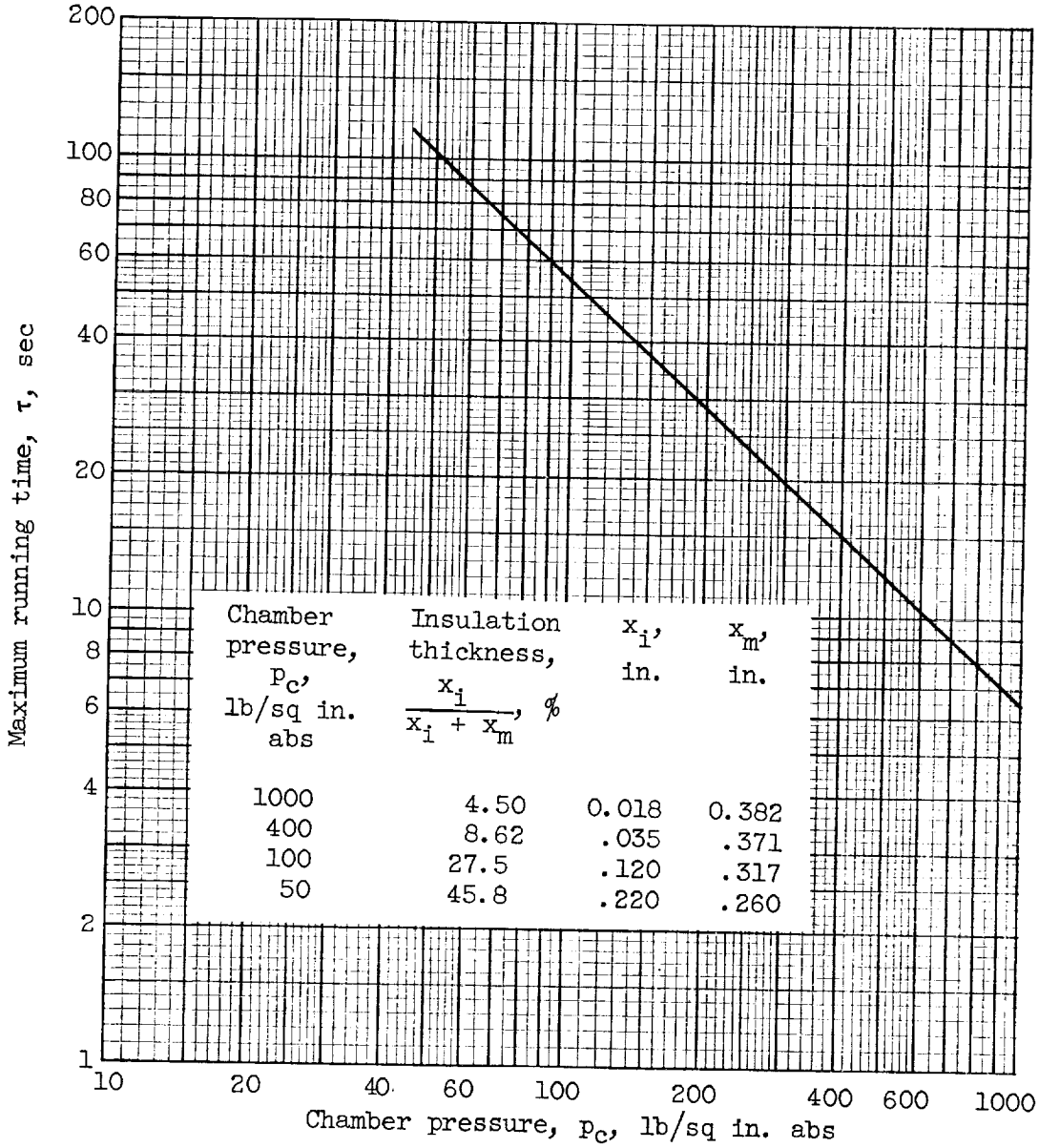

Figure 5. - Calculated effect of chamber pressure on maximum running time for nozzle throat for nominal 0.4-inch insulated wall. Gas temperature, 4660° F; wall weight, 0.1115 pound per square inch.

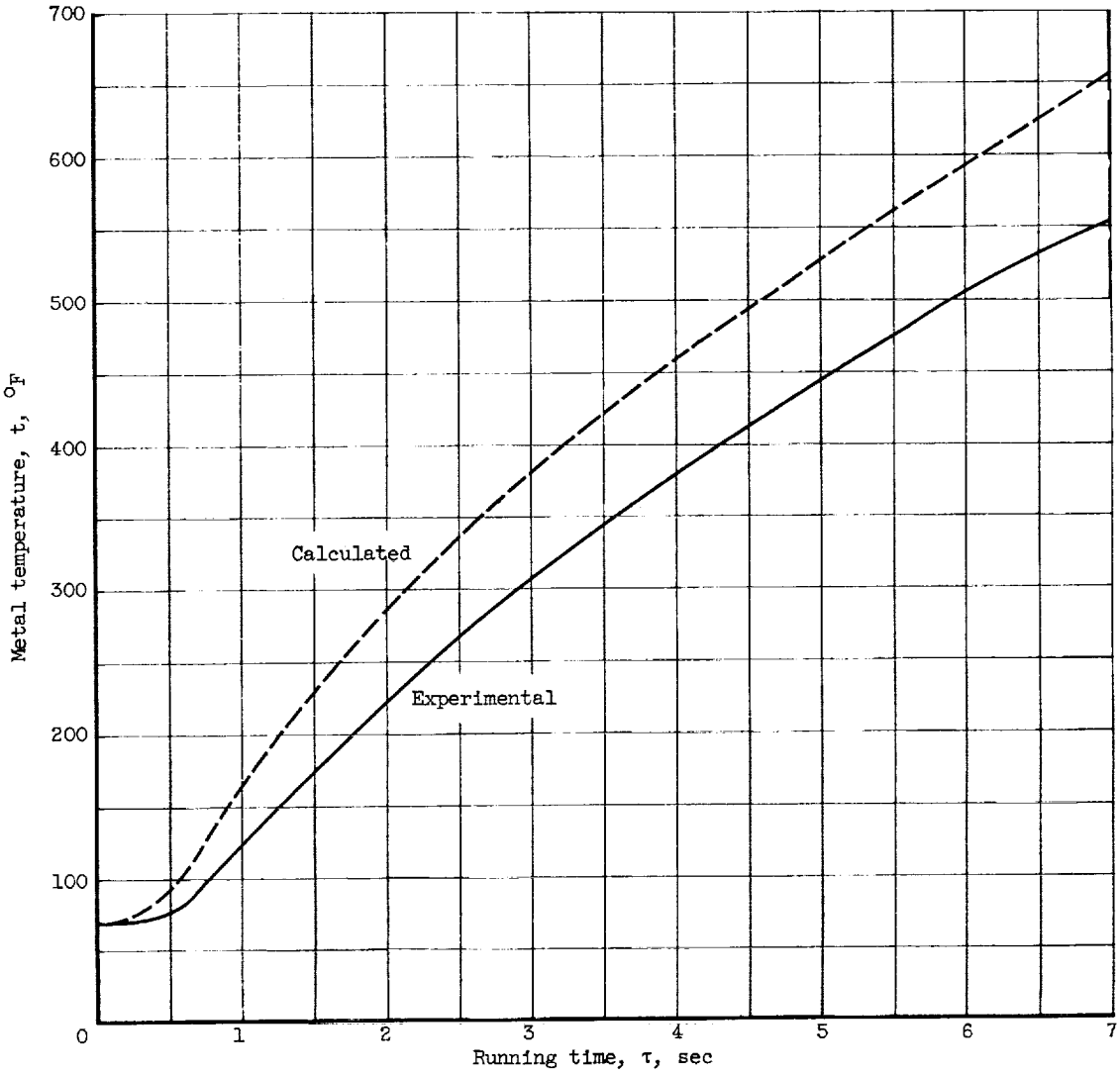

(a) Inner metal surface temperature. Measurement-station area ratio, A/A_t, 4.76; insulation thickness, x_i, 0.042 inch; base thickness, x_m, 0.355 inch; nozzle outside-to-inside-diameter ratio, d_o/d_{in}, 1.18; average chamber pressure, p_c, 973 pounds per square inch absolute.

Figure 6. - Comparison of typical calculated and measured temperature-time histories in steel nozzle wall insulated with zirconium oxide.

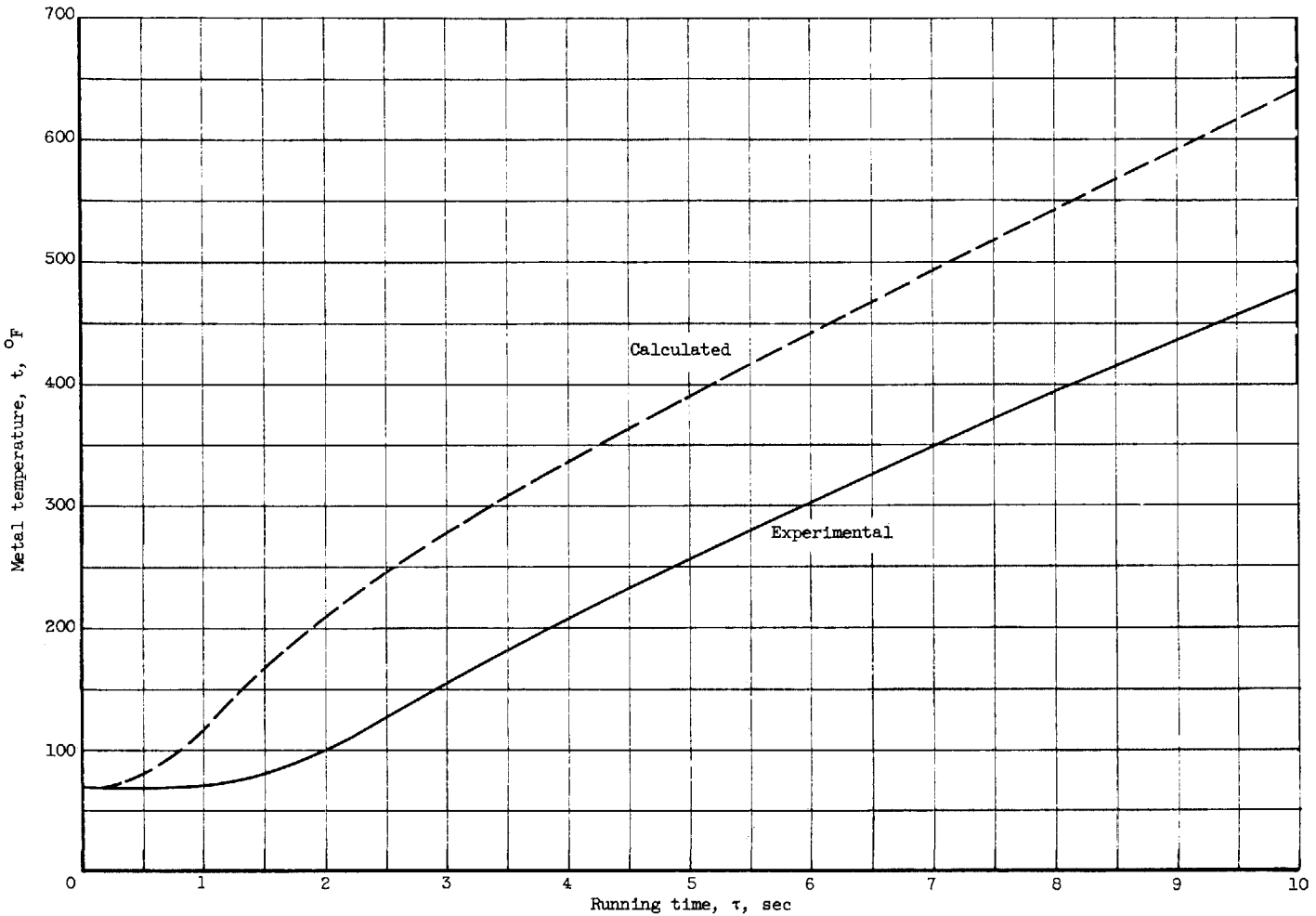

(b) Inner metal surface temperature. Measurement-station area ratio, A/A_t, 4.26; insulation thickness, x_i, 0.041 inch; base thickness, x_m, 0.356 inch; nozzle outside- to inside-diameter ratio, d_o/d_{in}, 1.163; average chamber pressure, p_c, 371 pounds per square inch absolute.

Figure 6. - Continued. Comparison of typical calculated and measured temperature-time histories in steel nozzle wall insulated with zirconium oxide.

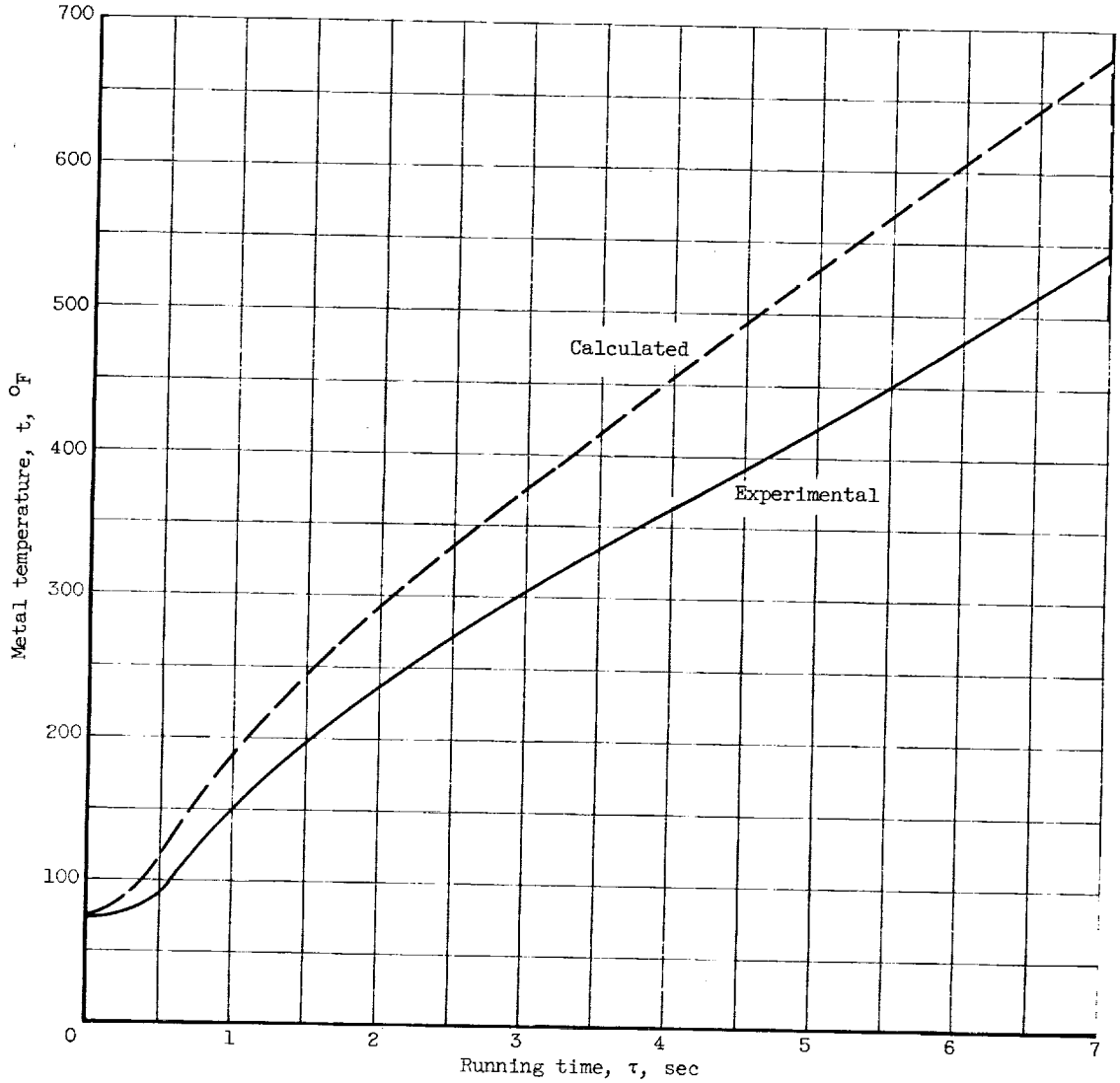

(c) Inner metal surface temperature. Measurement-station area ratio, A/A_t, 4.43; insulation thickness, x_i, 0.033 inch; base thickness, x_m, 0.353 inch; nozzle outside- to inside-diameter ratio, d_o/d_{in}, 1.135; average chamber pressure, p_c, 197 pounds per square inch absolute.

Figure 6. - Continued. Comparison of typical calculated and measured temperature-time histories in steel nozzle wall insulated with zirconium oxide.

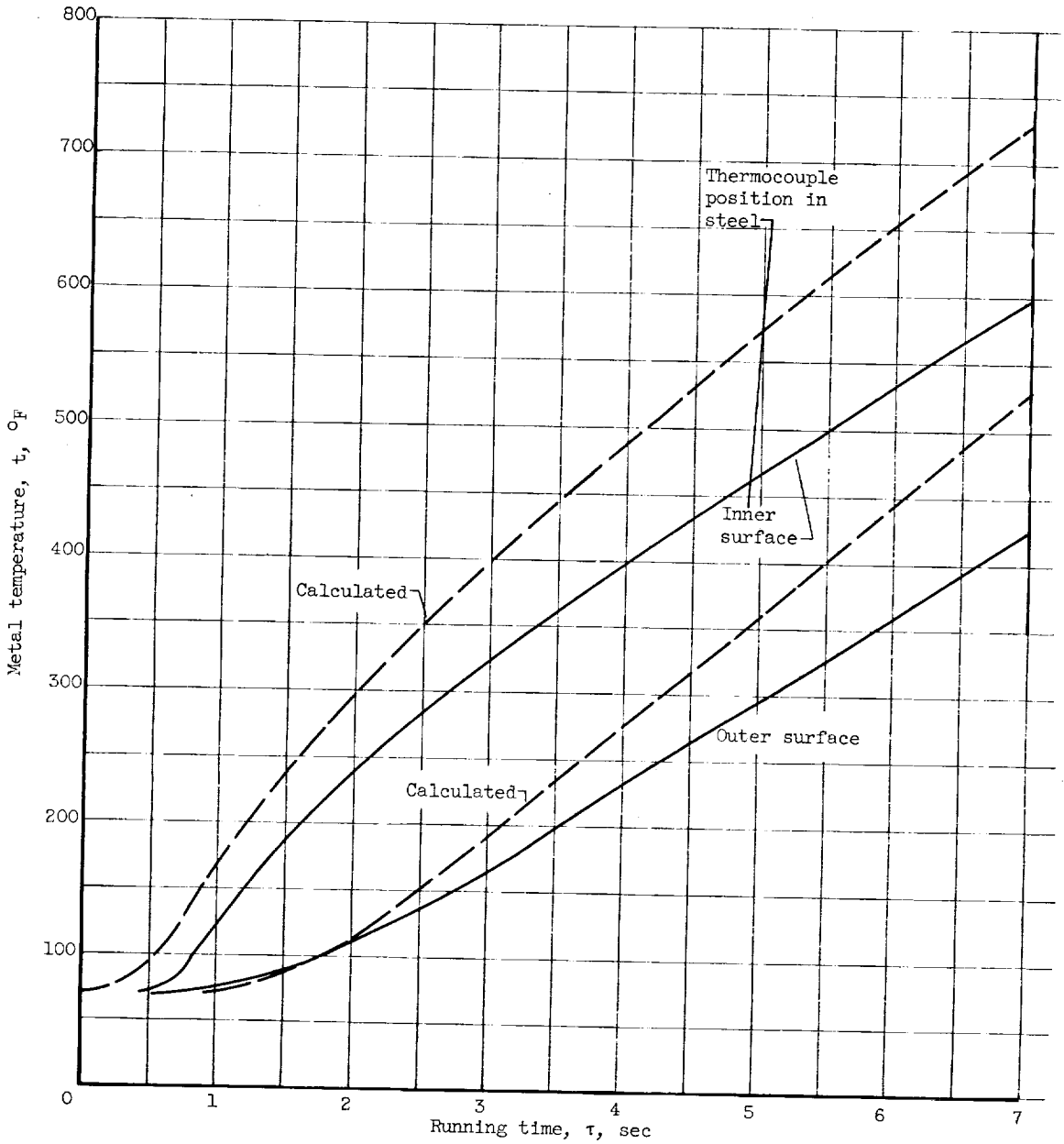

(d) Inner and outer metal surface temperatures. Measurement-station area ratio, A/A_t, 4.07; insulation thickness, x_i, 0.042 inch; base thickness, x_m, 0.30 inch; nozzle outside- to inside-diameter ratio, d_o/d_{in}, 1.17; average chamber pressure, p_c, 913 pounds per square inch absolute.

Figure 6. - Continued. Comparison of typical calculated and measured temperature-time histories in steel nozzle wall insulated with zirconium oxide.

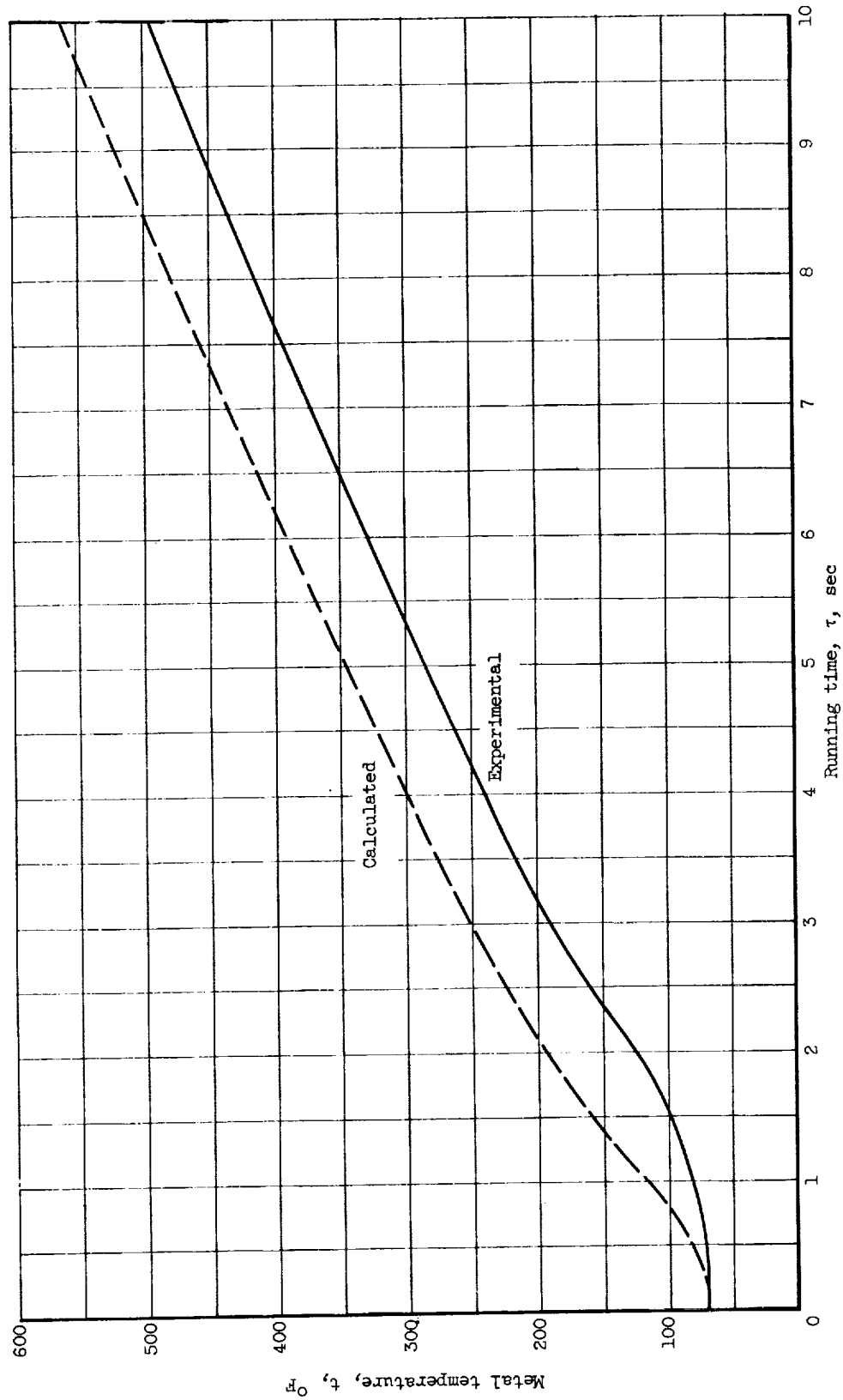

(e) Inner metal surface temperature. Measurement-station area ratio, A/A_t, 7.38; insulation thickness, x_1, 0.034 inch; base thickness, x_m, 0.340 inch; nozzle outside- to inside-diameter ratio, d_o/d_{in}, 1.1; average chamber pressure, p_c, 371 pounds per square inch absolute.

Figure 6. - Continued. Comparison of typical calculated and measured temperature-time histories in steel nozzle wall insulated with zirconium oxide.

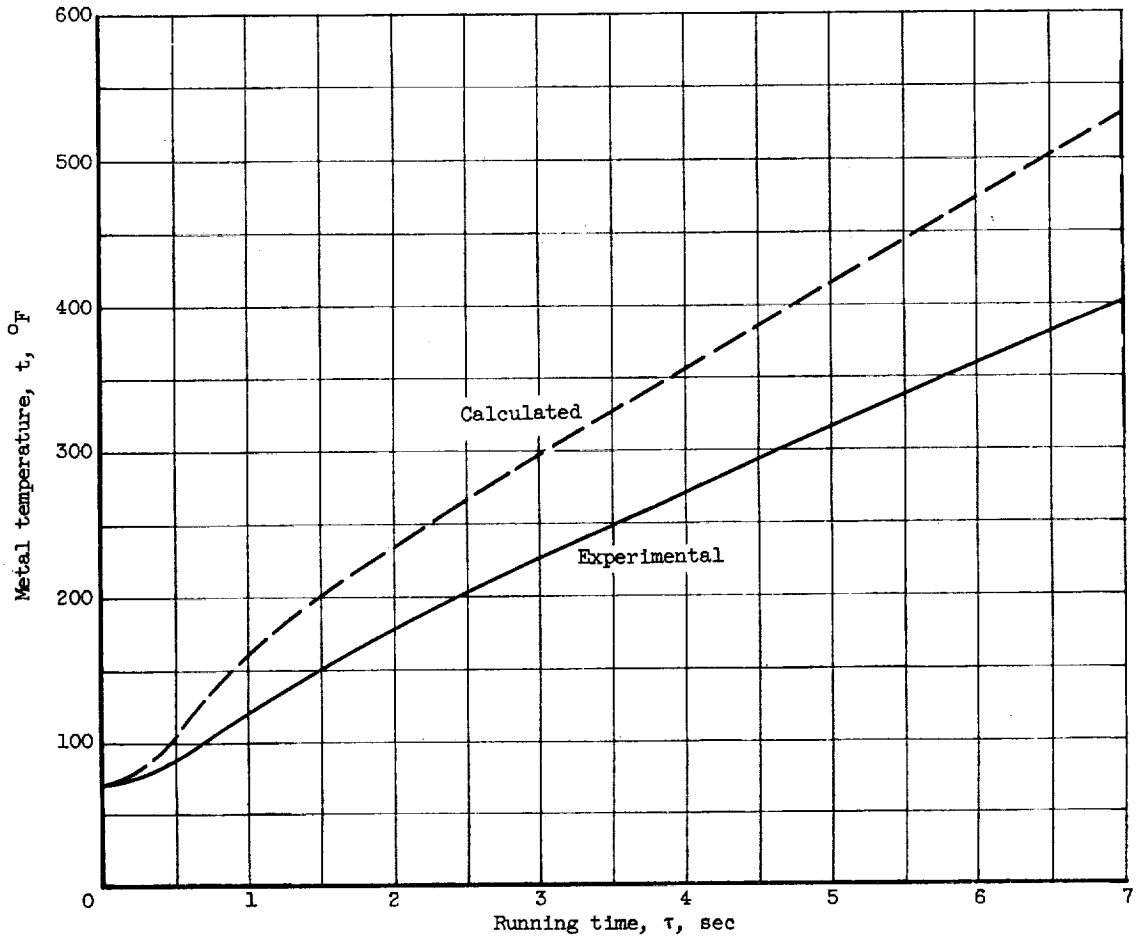

(f) Inner metal surface temperature. Measurement-station area ratio, A/A_t, 7.51; insulation thickness, x_i, 0.030 inch; base thickness, x_m, 0.359 inch; nozzle outside- to inside-diameter ratio, d_o/d_{in}, 1.097; average chamber pressure, p_c, 197 pounds per square inch absolute.

Figure 6. - Concluded. Comparison of typical calculated and measured temperature-time histories in steel nozzle wall insulated with zirconium oxide.